Chinese Chemical Letters 32 (2021) 1967–1971

Contents lists available at ScienceDirect

Chinese Chemical Letters

journal homepage: www.elsevier.com/locate/cclet

Communication

Signal-on bimodal sensing glucose based on enzyme product-etching MnO_2 nanosheets for detachment of MoS_2 quantum dots

Lingzhi Chen[a,1], Xueqin Huang[b,1], Xueyi Zeng[a], Guiting Fang[c], Weijian Chen[c], Haibo Zhou[d], Xing Zhong[c,*], Huaihong Cai[a,*]

[a] Department of Chemistry, College of Chemistry and Materials Science, Jinan University, Guangzhou 510632, China
[b] State Key Laboratory of Quality Research in Chinese Medicines, Macau University of Science and Technology, Macau 000583, China
[c] Department of Ultrasonography, The First Affiliated Hospital of Jinan University, Guangzhou 510632, China
[d] Institute of Pharmaceutical Analysis and Guangdong Province Key Laboratory of Pharmacodynamic Constituents of Traditional Chinese Medicine & New Drug Research, College of Pharmacy, Jinan University, Guangzhou 510632, China

ARTICLE INFO

Article history:
Received 24 August 2020
Received in revised form 11 January 2021
Accepted 13 January 2021
Available online 20 January 2021

Keywords:
MoS_2 quantum dots
MnO_2 nanosheets
Bimodal sensing
Glucose detection
Fluorescent/magnetic enhancement

ABSTRACT

The sensitive and rapid detection of blood glucose is very important for monitoring and managing diabetes. Herein, a fluorescent/magnetic bimodal sensing strategy is proposed for glucose detection using a multifunction-responsive nanocomposite (MoS_2 QDs-MnO_2 NS). MoS_2 QDs act as fluorescent probes, and MnO_2 nanosheets are used as both quenchers and recognizers in this sensing platform. In the presence of glucose-mediated enzyme product (H_2O_2), MnO_2 nanosheet is etched, thus releasing MoS_2 QDs and Mn^{2+} ions, which causes the significantly enhancement of fluorescent and magnetic signals. Furthermore, MoS_2 QDs-MnO_2 NS-based fluorescent test paper is constructed for H_2O_2 sensing with the naked eyes. Under optimal conditions, the dual linear ranges of 20–300 μmol/L and 40–250 μmol/L toward glucose detection are obtained for the fluorescent and magnetic mode, respectively. Furthermore, this bimodal assay exhibits good reproducibility and acceptable accuracy in glucose detection of clinical samples, demonstrating great versatility and flexibility of multifunctional probes in glucose detection.

Glucose is the important energy source in human body and plays the vital roles in human metabolism [1]. The rapid and sensitive detection of blood glucose is important for monitoring and managing diabetes [2,3]. Currently, different methods for glucose detection have been developed, including chemiluminescence [4], chromatography [5], electrochemistry [6], colorimetry [7] and fluorescence methods [8]. Most of these developed approaches are only used single-modal sensing strategy, while multi-modal glucose sensors that meet the clinical requirements are rare. The combination of fluorescence sensing with clinical imaging tools, such as magnetic resonance imaging (MRI), is significant not only for multi-modal sensing, but also for giving complementary diagnostic information with improving specificity, sensitivity, and accuracy [9]. Currently, manganese dioxide nanosheet (MnO_2 NS) has been widely used in fluorescence sensing owing to its large surface area and superior light absorption capability [10,11]. On the other hand, MnO_2 NS has a poor T_1-weighted MRI signal, whereas free Mn^{2+} ions have a strong MRI signal [9]. Although MnO_2-based sensors have been reported for bimodal detection of H_2O_2 using H_2O_2-induced decomposition of MnO_2 NS [12–14], there is no report about glucose assay using bimodal sensing strategy owing to the lack of a highly selective recognition approach. It is known that enzyme reactions produce H_2O_2 through the oxidation of glucose by glucose oxidase (GOx). Therefore, sensitive detection of glucose can be obtained by accurate detection of GOx-mediated enzyme product (H_2O_2) [15]. Considering these characteristics, we hypothesize that MnO_2 NS could be a useful material in constructing a fluorescent/magnetic bimodal sensor for glucose detection.

Molybdenum disulfide quantum dots (MoS_2 QDs) are superiors in this regard due to their advantages of tunable photoluminescence property, good photostability, and low biotoxicity [16]. Our previously study has shown that MoS_2 QDs have strong blue photoluminescence at 400 nm under UV irradiation [17]. Thereby, the MoS_2 QDs not only act as fluorescent nanoprobes for the fabrication of bimodal sensor, but also provide output signals for constructing fluorescent test paper [18].

Herein, we developed a fluorescent/magnetic bimodal sensing platform for quantitative detection of glucose using the MoS_2

* Corresponding authors.
E-mail addresses: tzhxing@jnu.edu.cn (X. Zhong), thhcai@jnu.edu.cn (H. Cai).
[1] These authors contributed equally to this work.

https://doi.org/10.1016/j.cclet.2021.01.030

QDs-MnO_2 NS nanocomposites. In this sensing strategy, fluorescence of MoS_2 QDs is effectively quenched by MnO_2 NS. In the presence of enzyme product of H_2O_2, produced by the redox reaction between glucose and GOx, MnO_2 could be reduced into Mn^{2+}, resulting in the recovery of QDs' fluorescence and enhancement in MRI signal. This switchable fluorescent/magnetic sensing platform is used for detecting blood glucose level in clinical samples. Additionally, MoS_2 QDs-MnO_2 NS-based fluorescent test paper is constructed for visual sensing of H_2O_2.

MnO_2 NS was synthesized by oxidation of $MnCl_2$ by H_2O_2 in the presence of tetramethylammonium hydroxide (TMA·OH) [19]. Results from high-solution transmission electron microscopy (HR-TEM) and atomic force microscopy (AFM) showed that the as-prepared MnO_2 NS has the sheetlike nanostructure (Fig. 1A and Fig. S1 in Supporting information), which would provide a large surface area for the adsorption of MoS_2 QDs. The energy-dispersive spectroscopy (EDS) analysis showed that the presence of Mn and O elements (Fig. S2A in Supporting information), verifying the successful synthesis of MnO_2 NS. HR-TEM imaging displayed the as-synthesized MoS_2 QDs were mono-dispersed with the average size of about 2−3 nm (Fig. 1B). The EDS analysis confirmed the presence of Mo and S elements (Fig. S2B in Supporting information). HR-TEM image of MoS_2 QDs-MnO_2 NS nanocomposite confirmed that MoS_2 QDs dispersed homogeneously on MnO_2 NS surface (Fig. 1C). The crystal lattice *d*-spacing (inset of Fig. 1C) was identified to be 0.2 nm, which corresponded to the (100) lattice plane of MoS_2 crystal [20]. The correspondingly EDS analysis demonstrated the presence of Mn, Mo, and S elements (Fig. S3 in Supporting information), verifying the successful synthesis of MoS_2 QDs-MnO_2 NS. The zeta potential measurement showed that MnO_2 NS had a negative ζ-potential value of −28.2 mV, MoS_2 QDs possessed a ζ-potential value of −13.6 mV. Thus, MoS_2 QDs-MnO_2 NS nanocomposites are constructed by the physical adsorption of MoS_2 QDs on nanosheet surface.

The optical properties of MoS_2 QDs, MnO_2 NS and MoS_2 QDs-MnO_2 NS nanocomposites were characterized, as illustrated in Fig. 1. MoS_2 QD solution showed a strong fluorescent signal at 400 nm (Fig. 1D). Their fluorescence behaviors had no obvious change in the presence of highly H_2O_2 concentration (Fig. S2C in Supporting information), demonstrating QDs have good photostability. UV–vis absorption spectrum of MnO_2 NS exhibited a wide band at 200−800 nm, which was well-overlapped with the emission spectrum of MoS_2 QDs (Fig. 1D), showing MnO_2 NS could effectively quench fluorescence of MoS_2 QDs *via* Förster resonance energy transfer (FRET). Fig. 1E confirmed MnO_2 NS could induce fluorescence quenching. Fluorescence of QDs was significantly decreased after the formation of MoS_2 QDs-MnO_2 NS nanocomposites. As shown in Fig. 1F, about 90% of fluorescence is quenched after addition of 300 μmol/L MnO_2 NS, and then fluorescent signal reaches to be stable. Thus, 300 μmol/L of MnO_2 NS is chosen for the construction of MoS_2 QDs-MnO_2 NS nanocomposites. Additionally, the reaction time between MoS_2 QDs and MnO_2 NS was quick (only 1 min) (Fig. S2D in Supporting information). These results demonstrate that MoS_2 QDs-MnO_2 NS nanocomposites have the fluorescence "turn off" signal. The designed strategy for bimodal glucose sensing is based on the oxidation of MnO_2 by H_2O_2 ($MnO_2 + H_2O_2 + 2H^+ \rightarrow Mn^{2+} + 2H_2O + O_2$) [9], and H_2O_2 can be acquired by GOx through the catalytic oxidization of glucose. To clarify this, different characterization methods are used, as shown in Fig. 2. Compared with MoS_2 QDs-MnO_2 NS, a strong fluorescence enhancement was observed after the addition of H_2O_2 (Fig. 2A). The interaction between MoS_2 QDs-MnO_2 NS and H_2O_2 was further characterized by HR-TEM. As shown in Fig. 2B, the nanosheets are etched and the adsorbed MoS_2 QDs are released. This demonstrates H_2O_2-triggered decomposition of MnO_2 NS can weaken QDs' adsorption, resulting in switchable fluorescence "turn off-on". We therefore used MoS_2 QDs-MnO_2 NS for glucose sensing. In the presence of glucose and GOx, fluorescent signal was increased by 9 times than that of MoS_2 QDs-MnO_2 NS (Fig. 2A). This shows that fluorescence "off-on" sensing of glucose is feasible.

Along with fluorescence recovery, the T_1-weight magnetic imaging for MoS_2 QDs-MnO_2 NS was significantly lightened after introducing of GOx-mediated enzyme product (H_2O_2) (Inset of Fig. 2A), demonstrating the positive correlation between MRI signal and glucose sensing. This is ascribed to a high T_1-weight contrast signal of Mn^{2+} ions, resulting from the oxidation of MnO_2 by H_2O_2 [9]. In the absence of glucose, both fluorescence and MRI signals are silent. However, fluorescence recovery and MRI enhancement are obtained after introducing of glucose and GOx,

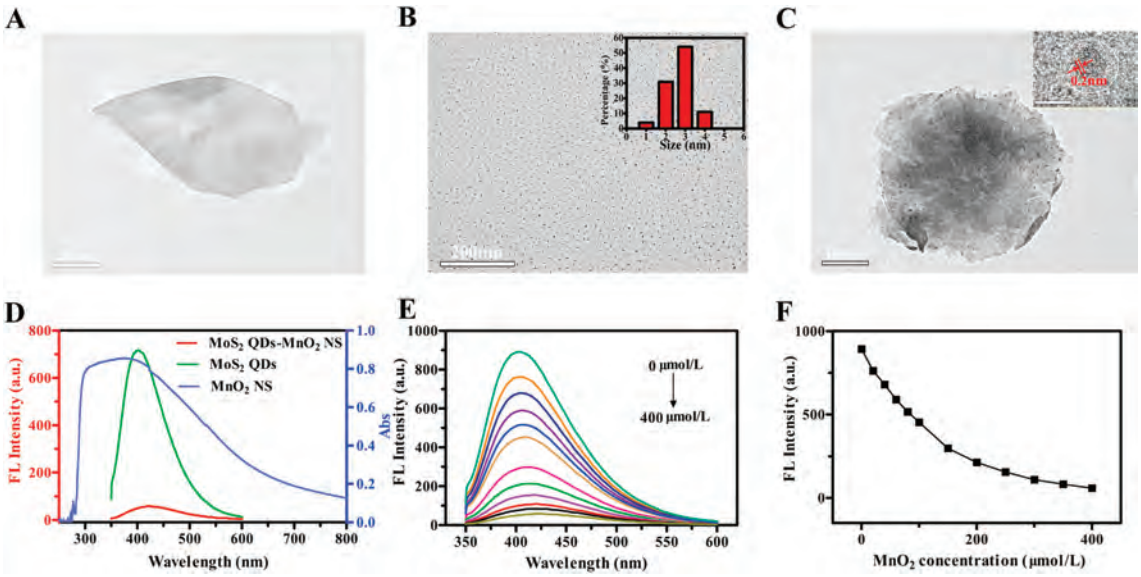

Fig. 1. (A–C) HR-TEM images of MnO_2 NS (A), MoS_2 QDs (B), MoS_2 QDs-MnO_2 NS nanocomposite (C). (D) UV–vis absorption spectrum of MnO_2 NS, fluorescence spectra of MoS_2 QDs and MoS_2 QDs-MnO_2 NS. (E) Influence of MnO_2 NS concentration on the preparation of MoS_2 QDs-MnO_2 NS. (F) The optimal concentration of MnO_2 NS.

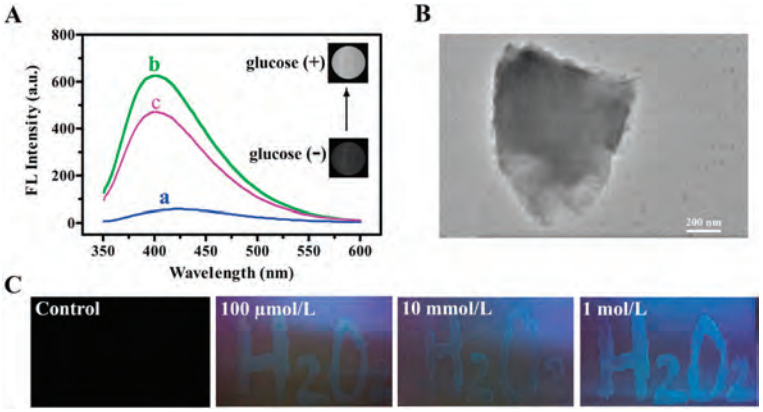

Fig. 2. (A) Fluorescence spectra of MoS_2 QDs-MnO_2 NS (a), MoS_2 QDs-MnO_2 NS + H_2O_2 (200 μmol/L) (b), MoS_2 QDs-MnO_2 NS + GOx (0.6 mg/mL) + glucose (400 μmol/L) (c); Inset: T_1-weighted magnetic images of MoS_2 QDs-MnO_2 NS in the absence or presence of glucose (400 μmol/L) + GOx (0.6 mg/mL). (B) HR-TEM image of MoS_2 QDs-MnO_2 NS interacting with 200 μmol/L H_2O_2. (C) Visualization of H_2O_2 sensing using MoS_2 QDs-MnO_2 NS-based fluorescent test papers, fluorescence photographs were taken under UV irradiation.

showing the "light on" signals for bimodal sensing. These results show that MoS_2 QDs-MnO_2 NS can be used to detect glucose through fluorescent/magnetic bimodal strategy.

Fluorescent test paper is an attractive tool for rapid identification and sensing of analytes through visual observation of fluorescence change [21], which has advantages of rapid recognition, easy operation and low cost. Recently, fluorescent test papers have been constructed by assembling or printing fluorescent probes on a piece of membrane-based substrates [22]. Although QDs-based test papers were explored to detect the explosives [23] and heavy metal ions [24], however, MoS_2 QDs-MnO_2 NS-based test paper used for visual H_2O_2 sensing has not been reported. Herein, different concentrations of H_2O_2 solutions as "ink" were written on MoS_2 QDs-MnO_2 NS-immersed microporous membrane. When H_2O_2 was not "written", test paper displayed non-fluorescent signal under UV irradiation (Fig. 2C). When H_2O_2 solution (100 μmol/L) was evenly written on test paper, the weak blue fluorescence from a word "H_2O_2" was observed under UV irradiation, showing visual identification of H_2O_2 (Fig. 2C). A high-concentration H_2O_2 (such as 10 mmol/L and 1 mol/L) caused an increasing brightness in blue fluorescence, which was consistent with our proposed mechanism. Although the accurate quantitative assay is not achieved, the variations in fluorescence brightness provide semi-quantitatively identification of H_2O_2.

In order to optimize analytical performance, the optimal experiment conditions are investigated, including GOx concentration, pH value, the reaction time, and interaction temperature. Generally, GOx concentration directly affects H_2O_2 production, correspondingly, influences the sensitivity of assay. Fluorescent intensity of MoS_2 QDs initially increased with increasing GOx concentration, and then reached a plateau (Fig. S4A in Supporting information). This indicates that higher concentration of GOx leads to much more H_2O_2 production. The maximum fluorescent intensity is achieved at 0.6 mg/mL GOx, which is selected as the optimal GOx concentration in following experiments. The reaction time between MoS_2 QDs-MnO_2 NS and enzyme product (H_2O_2) affects the detection signals. Fluorescent intensity of MoS_2 QDs-MnO_2 NS increased initially and then tended to be stable after 30 min (Fig. S4B in Supporting information). Therefore, the 30-min time is selected for the interacting time. Reaction temperature also can affect the activity of enzyme reaction. When reaction temperature increased to a critical point (37 °C), the maximal fluorescence intensity was obtained (Fig. S4C in Supporting information). This demonstrates the optimal reaction temperature would effectively promote the enzymatic reaction, resulting in higher amount of H_2O_2 production. Therefore, the optimal reaction temperature for glucose sensing is 37 °C. It is known that pH value greatly affects the enzyme reaction, correspondingly, influences the sensitivity of detection signals. Fluorescent intensity initially increased and then reached the maximum at the pH value of 5.0 (Fig. S4D in Supporting information). However, when pH was higher than 5.0, an obvious decrease in the fluorescent intensity was observed. Therefore, the buffer solution at pH 5.0 is used in this enzymatic reaction.

Under optimal experimental conditions (Fig. S4 in Supporting information), a novel signal-on bimodal assay was performed for glucose detection. Fig. 3A shows that fluorescent intensity of MoS_2 QDs-MnO_2 NS enhanced with the increasing concentration of glucose. A good linear relationship was obtained between the magnitude of (F-F_0) from MoS_2 QDs-MnO_2 NS and glucose concentrations in the range of 20−300 μmol/L. A linear regression equation was fitted to $F\text{-}F_0 = 137.88 + 1.33C_{glucose}$ ($R^2 = 0.991$) (Fig. 3B), and the limit of detection (LOD) was calculated to be 4.9 μmol/L on the basis of the equation of $3\sigma/S$ (σ is the standard deviation of the blank samples; S is the slope of the calibration curve), showing good sensitivity in comparison with other glucose detection method (Table S1 in Supporting information). This MoS_2 QDs-MnO_2 NS-based sensing platform has some advantages including no chemical modification, simpler assay steps, low background signal, and bimodal quantitative analysis. In order to determine the specificity of the MoS_2 QDs-MnO_2 NS for sensing glucose, interfering agents, including Na^+, Ca^{2+}, Zn^{2+}, maltose, fructose, glutathione (GSH), and cysteine (Cys), were examined under the same detection conditions. The MoS_2 QDs-MnO_2 NS showed a remarkable fluorescence change toward glucose, while some interfering agents induced negligible changes, including Na^+, Ca^{2+}, Zn^{2+}, maltose, and fructose (Fig. 3C). However, GSH and Cys, which may coexist in human serum, could enhance fluorescence intensity, resulting from the redox reaction between MnO_2 and GSH or Cys. This interference can be effectively eliminated by adding *N*-ethylmaleimide (NEM), a thiol scavenger, which specifically reacts with GSH or Cys, but not reacts with glucose [25]. As we expected, MoS_2 QDs-MnO_2 NS showed a lower signal when serum samples were pre-added with NEM (Fig. 3C). Therefore, MoS_2 QDs-MnO_2 NS provides a selective and sensitive approach for blood glucose detection after pre-treatment in human serum samples.

For magnetic sensing of glucose, magnetic signals of MoS_2 QDs-MnO_2 NS were investigated in the presence of glucose-mediated enzyme product (H_2O_2). As shown in Fig. 3D, the longitudinal relaxation rates ($1/T_1$) enhances with the increasing concentration

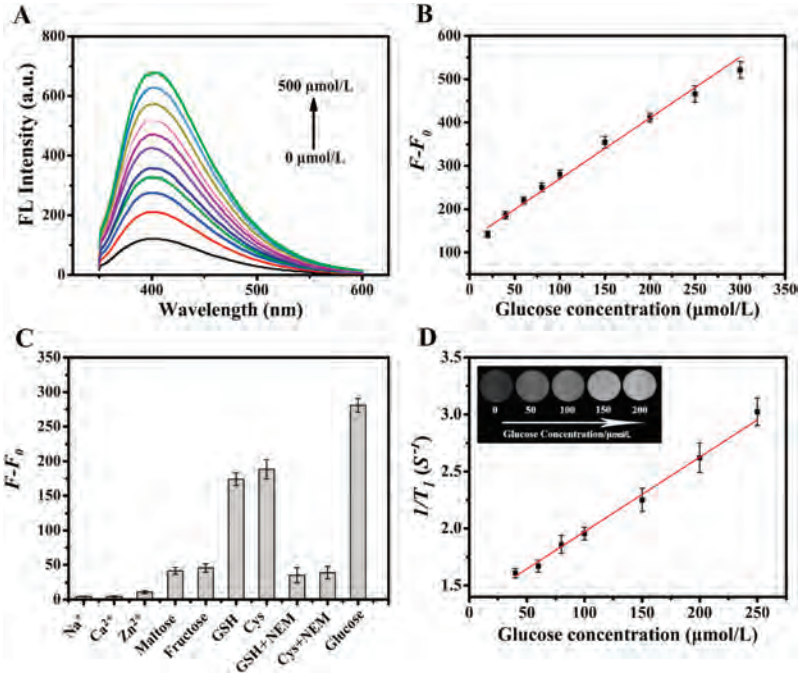

Fig. 3. (A) Fluorescent response of MoS_2 QDs-MnO_2 NS in the presence of different concentration of glucose and 0.6 mg/mL GOx. (B) The calibration curve of (F-F_0) *vs.* glucose concentration (F and F_0 are fluorescence intensities of MoS_2 QDs-MnO_2 NS in the presence or absence of glucose, respectively). (C) The specificity of this sensing platform under different interfering substances (0.3 mmol/L), NEM (0.9 mmol/L). (D) The calibration curve of $1/T_1$ *vs.* glucose concentration (Inset: T_1-weight magnetic images of MoS_2 QDs-MnO_2 NS under glucose-induced H_2O_2 product).

of glucose in the range of 40−250 μmol/L. A linear regression equations of $1/T_1 = 1.30 + 0.067\ C_{glucose}$ ($R^2 = 0.994$) was fitted, and the LOD was calculated to be 40 μmol/L on the basis of the equation of $3\sigma/S$ (σ is the standard deviation of the blank samples; S is the slope of the calibration curve). Furthermore, the brightness of MRI imaging increased obviously (inset of Fig. 3D), visually showing the enhancement of magnetic signal resulted from H_2O_2-mediated Mn^{2+} production.

Sensitive and selective sensing of glucose in clinical samples is highly important for clinical diagnosis and therapeutic guidance. Encouraged by the excellent fluorescent response to glucose detection in solution, the developed method was further applied to detect blood glucose level in human serum samples, including the healthy, the diabetic patients, and the diabetic patients treated by the hypoglycemic drug. Herein, human serum samples containing glucose and spiked samples were chosen for these experiments. Considering the interferences resulted from Cys or GSH in serum, serum samples were pretreated with 50 μL of NEM (0.3 mmol/L) for reacting 10 min to remove these interferences. Thereafter, these pre-treated samples were determined by using MoS_2 QDs-MnO_2 NS-based fluorescent assay and a commercial automatic glucose analyzer, respectively. Because the normal blood glucose level in healthy is 3.9–6.1 mmol/L [2], human serum samples are diluted to make glucose concentrations in the linear range of our proposed method. Using our strategy, glucose concentrations from the healthy were in the range of 4.5–5.2 mmol/L, however, glucose levels increased to the range of 6.7–14.2 mmol/L in diabetic patients (Table 1). When the diabetic patients were treated with hypoglycemic drug, the glucose level significantly decreased to 5.5 mmol/L (Table 1), which was closed to the normal glucose level. These results have a good agreement with the obtained from a commercial automatic glucose analyzer (Table 1). In addition, the standard spiked experiments were also carried out. The recoveries ranged from 96.2% to 104.8% for the above six real samples, and RSD ranging from 3.7% to 5.6% were obtained. These results show the accuracy of our proposed method is acceptable.

In summary, this work demonstrates bimodal sensing for glucose and visual identification of H_2O_2 by coupling with fluorescent/magnetic responses of MoS_2 QDs-MnO_2 NS and MnO_2-mediated H_2O_2 etching interaction. This dual-modal

Table 1
Comparison of results from MoS_2 QDs-MnO_2 NS-based fluorescent assay and a commercial automatic glucose analyzer for evaluation method accuracy in glucose detection[a]

Samples	Clinical serum samples containing glucose		Spiked glucose in clinical serum samples		
	Our proposed method	Automatic glucose analyzer	Spiked	Found	Recovery
1	5.2% ± 3.4%	5.6% ± 2.1%	5.0	10.1% ± 3.7%	98.4%
2	4.5% ± 2.9%	5.1% ± 1.5%	5.0	9.3% ± 4.3%	96.6%
3	6.7% ± 4.2%	6.6% ± 1.7%	5.0	12.2% ± 4.8%	104.8%
4	11.5% ± 3.4%	11.2% ± 2.5%	5.0	16.3% ± 5.4%	103.2%
5	14.2% ± 4.0%	14.5% ± 2.8%	5.0	18.9% ± 5.6%	96.2%
6	5.5% ± 4.7%	5.1% ± 1.8%	5.0	10.5% ± 4.6%	102.2%

[a] Samples 1–6 are the clinical samples. Samples 1 and 2 are the healthy, samples 3–5 are diabetic patients, and sample 6 is the diabetic patient treated by the hypoglycemic drug. All data as mean ± RSD are obtained on the basis of three measurements.

sensing strategy provides more advantages than the single sensing mode. Additionally, MoS_2 QDs-MnO_2 NS-based fluorescent test papers could semi-quantitatively evaluate H_2O_2 level basing on the color change. These results provide a potential application of bimodal sensing in chemical analysis and clinical diagnostics.

Declaration of competing interest

The authors declare that they have no known competing financial interests or personal relationships that could have appeared to influence the work reported in this paper.

Acknowledgments

This work is financially supported by the Natural Science Foundation of Guangdong Province (No. 2018A0303130002), the National Natural Science Foundation of China (No. 81773684), Guangdong Natural Science Funds for Distinguished Young Scholars (No. 2018B030306033), Pearl River Talent Program (No. 2017GC010363), and Pearl River S&T Nova Program of Guangzhou (No. 201806010060).

Appendix A. Supplementary data

Supplementary material related to this article can be found, in the online version, at doi:https://doi.org/10.1016/j.cclet.2021.01.030.

References

[1] X.Y. Lin, Y.F. Wang, M.M. Zou, T.X. Lan, Y.N. Ni, Chin. Chem. Lett. 30 (2019) 1157–1160.
[2] G.B. Mao, Q. Cai, F.B. Wang, et al., Anal. Chem. 89 (2017) 11628–11635.
[3] A. Liu, M.M. Li, J.X. Wang, et al., Chin. Chem. Lett. 31 (2020) 1133–1136.
[4] H.J. Li, C.L. Liu, D. Wang, C.S. Zhang, Biosens. Bioelectron. 91 (2017) 268–275.
[5] W.Q. Xie, Y.X. Gong, K.X. Yu, J. Chromatogr. A 1520 (2017) 143–146.
[6] A.A. Llobregata, I. Jeerapanb, A. Bandodkarb, et al., Biosens. Bioelectron. 91 (2017) 885–891.
[7] Y.N. Qin, Y.J. Sun, Y.J. Li, et al., Chin. Chem. Lett. 31 (2020) 774–778.
[8] J.L. Ma, B.C. Yin, X. Wu, B.C. Ye, Anal. Chem. 89 (2017) 1323–1328.
[9] J.P. Sheng, X.X. Jiang, L.Q. Wang, M.G. Yang, Y.N. Liu, Anal. Chem. 90 (2018) 2926–2932.
[10] J.Q. Qin, Z.S. Wu, F. Zhou, et al., Chin. Chem. Lett. 29 (2018) 582–586.
[11] C. Peng, H.H. Xing, X.S. Fan, et al., Anal. Chem. 91 (2019) 5762–5767.
[12] H.R.H. Ali, A.I. Hassan, Y.F. Hassanb, M.M. El-Wekil, RSC Adv. 10 (2020) 17506–17514.
[13] J.L. Chen, L. Li, S. Wang, et al., J. Mater. Chem. B Mater. Biol. Med. 5 (2017) 5336–5344.
[14] R.C. Lv, M. Feng, L.Y. Xiao, et al., ACS Appl. Bio Mater. 1 (2018) 1505–1511.
[15] L.H. Fu, C. Qi, J. Lin, P. Huang, Chem. Soc. Rev. 47 (2018) 6454–6472.
[16] H. Zhu, H. Zhang, Y.S. Xia, Anal. Chem. 90 (2018) 3942–3949.
[17] X. Tang, X.Y. Zeng, H.M. Liu, et al., Microchim. Acta 186 (2019) 572–584.
[18] Y.L. Xu, X.Y. Niu, H.L. Chen, S.G. Zhao, X.G. Chen, Chin. Chem. Lett. 28 (2017) 338–344.
[19] T. Xiao, J. Sun, J.H. Zhao, et al., ACS Appl. Mater. Interfaces 10 (2018) 6560–6569.
[20] Z.X. Gan, Q.F. Gui, Y. Shan, et al., J. Appl. Phys. 120 (2016) 104503–104507.
[21] Q.S. Mei, Z.P. Zhang, Angew. Chem. Int. Ed. 51 (2012) 1–6.
[22] Y.J. Zhou, X.Y. Huang, C. Liu, et al., Anal. Chem. 88 (2016) 6105–6109.
[23] K. Zhang, H.B. Zhou, Q.S. Mei, et al., J. Am. Chem. Soc. 133 (2011) 8424–8427.
[24] C. Yuan, B.H. Liu, F. Liu, M.Y. Han, Z.P. Zhang, Anal. Chem. 86 (2014) 1123–1130.
[25] H. Ma, X.Y. Liu, X.D. Wang, et al., Microchim. Acta 184 (2017) 177–185.